Journal of the European Ceramic Society 22 (2002) 1191–1203

www.elsevier.com/locate/jeurceramsoc

On a way to material models for ceramics

Michel Coster, Jean-Louis Chermant*

LERMAT, URA CNRS 1317, ISMRA, 6 bd Maréchal Juin, 14050 Caen Cedex, France

Received 8 May 2001; received in revised form 28 August 2001; accepted 19 September 2001

This paper is dedicated to Professor Georges Matheron who passed away on 7 August 2000

Abstract

This paper presents different probabilistic models which are based (i) for monophased materials on closed random sets (RACSs) and space tessellation such as Voronoi, Johnson-Mehl or Poisson mosaic, and (ii) for polyphazed materials on topologically closed random sets such as Matheron's Boolean model, dead-leaves model, tessellation of polyphazed structures and Stienen's model. Examples are given in both cases, such as UO_2, Fe–Ag, TiC–Co, WC–Co, concrete... © 2002 Published by Elsevier Science Ltd.

Keywords: Microstructure; Modelling; Probabilistic models; Tessellations; Closed random sets; Matheron's Boolean models

1. Introduction

Properties of materials will depend on their morphology, which often is in turn governed by the manufacturing processes, so these three components are completely related all together. To control from all points of view a material, their relationships must be established. From a general point of view, it is, in fact, extremely complex and such a problem must be simplified. Some properties will depend mainly on morphological characteristics at the atomic scale, while others will be mainly influenced by the morphologies at the micronic scale.

In the case of ceramics, due to their very high sensitivity to defects and of their physical properties to morphological characteristics, their morphology has to be determined by accurate and statistical methods. Then the technique of automatic image analysis appear well suited,[1–3] but statistical measurements can be very time consuming. Moreover, these characteristics must correspond to 3D parameters, which is not always the case, for example the knowledge of the number of particles per unit volume requires serial sectioning.

Therefore, it is of interest to develop models for many reasons: (i) it can permit prediction of changes in the physical response of a ceramic or any other material from the changes in its microstructure,[4] (ii) it can be used in numerical simulations to better understand a behavior, for example of UO_2 or MOX ceramics under specific solicitations (nuclear ones);[5] (iii) it can reproduce realizations of microstructure in three dimensions; (iiii) it can allow accession to the best microstructure for a given characteristic or application that can be revealed from the correlations between morphological characteristics and physical, chemical, mechanical, ... ones determined from these models; (iiiii) if probabilistic models are used, it can allow easy access to any 3D morphological parameters (without the use of serial sectioning).

Presently, many types of models to simulate microstructures are developed, based on probability distributions, random-number generators, random variates, ... Monte Carlo process,... .[6,7]

The aim of this paper is to focuss only on probabilistic models[8] which can be easily implemented by the technique of automatic image analysis. On the one hand, it will be necessary to select a material enough simple (model material) with a microstructure which can be described without too much difficulties. On the other hand, one can suggest a morphological model to describe this microstructure (material model). These models will be set probabilistic models defined in $\mathbb{R}^2$ or, which will be better, in $\mathbb{R}^3$.

The modeling presents a certain number of advantages with regard to the classical description of a material:

* Corresponding author. Tel.: +33-231-452-664; fax: +33-231-452-660.

E-mail address: chermant@labolermat.ismra.fr (J.-L. Chermant).

0955-2219/02/$ - see front matter © 2002 Published by Elsevier Science Ltd.
PII: S0955-2219(01)00455-1

- the number of necessary parameters to describe completely the morphology is small,
- a simulation can be considered as to virtually construct the microstructure.

The modeling is not only applied to investigate the morphology of bulk materials.[8–14] It can also be used to characterize external morphologies such as non planar surfaces (fractures,...) or external surfaces of powders and divided materials (such as powders).[15–18] Two ways are possible: (i) the first one is an extension of the set probabilistic models towards probabilistic functions generally defined in $\mathbb{R}^2 \times \mathbb{R}$; (ii) the second one is based on fractals.[19] Only the first one will be approached in this paper.

2. Material Models, the Probabilistic Models

2.1. The frame of probabilistic models

To observe a morphology requires that a set X does not fill all the space. So there will be a minimum of two components in the medium investigated, the set X and its complementary X^c. The objects of this set can be as well points as straight lines or any sub-sets. Then the obtained set X will be a topologically closed random set (RACS, random closed set).[1,2,20,21] This restriction is important to preserve correct properties, but which are not embarrassing in practice. Thus a RACS will remain a RACS after an operation of erosion, dilation, ...

The choice of a model will depend on a certain a priori knowledge. In the case of bulk materials, the number of phases morphologically discernible is the first point. So there will be two main classes of materials, the monophased materials which will be described from a space tessellation, and the polyphazed materials from polyphazed RACS. Inside these two classes, other elements will must be taken into consideration as the shape, the dispersion, the size distribution, ...

2.1.1. Choquet's capacity

A RACS can be characterized by a probability of events corresponding to morphological measures such as the probability of inclusion of a compact K in a set or its complementary. It is the role attributed to the Choquet's capacity, $T(K)$, defined by:[1,20,22]

$$T(K) = \Pr(X \cap K \neq \varnothing) \tag{1}$$

$T(K)$ can also be defined from the probability Q(K) that the intersection between X and K is empty,

$$\mathrm{Q}(K) = 1 - T(K) = 1 - \Pr(X \cap K \neq \varnothing) = \Pr(K \subset X^c) \tag{2}$$

As for a distribution function which defines a random variable, the knowledge of the Choquet's capacity for any compact K allows to define completely a probabilistic model. It is evident that all the possible compacts cannot be tested. So the most simple ones will be used.

2.1.2. Properties of the RACS

The RACS can or cannot verify some properties,

- The *infinity divisibility*: A RACS X is infinitely divisible if X is equivalent to the union of n independent RACSs of same type. The intersection of a model infinitely divisible by a sub-space preserves the type of the generated model. That constitutes a stereological characteristic. For a such RACS and a given compact K, the Choquet's capacity is given by:

$$Q(K) = 1 - T(K) = \exp(-\Psi(K)) \text{ with } \Psi(\varnothing) = 0 \tag{3}$$

- *Stability*: An infinitely divisible RACS is stable by union if the function Ψ verifies the following expression:

$$\Psi(\lambda K) = \lambda^{\alpha}\Psi(K) \text{ with } \lambda > 0, \alpha > 0 \tag{4}$$

It describes an internal self-similarity which is not necessarily fractal.

- *Calculability*: A RACS possesses the property of calculability if for certain compacts K, the Choquet's capacity have explicit expressions. That will allow to verify if real structure can correspond to the realization of a RACS without carrying a simulation.

  When the Choquet's capacity is not calculable, characteristical magnitudes related to the parameters of the model can be used.

2.2. Point Poisson process

The starting point of any probabilistic model is a point Poisson process. The simplest process is the binomial one. It corresponds to a uniform distribution of n points in a set Z defined in $\mathbb{R}^n$. Nevertheless, one can note that the number of points belonging to a sub-set Z_1 is not independent from that in Z_2. That leads us to exclude this process to construct RACSs.

As the point Poisson process has not the same properties as the binomial law, it is preferable to use a point Poisson process rather than a binomial law. The probability that n points of a Poisson process of density θ belongs to a set Z is given by:

$$\Pr(Z) = \frac{[\theta \mathrm{mes}(Z)]^n}{n!} \exp(-\theta \mathrm{mes}(Z)) \tag{5}$$

This process is the base of derived models such as cluster and hard core ones.[13]

2.3. Models for random tessellation of space

The models for random tessellation are sets that cut the $\mathbb{R}^n$ space in several closed and bounded sub-sets called classes. The unions of all these sub-sets fill all the $\mathbb{R}^n$ space.

The main tessellation models are: the Voronoi tessellation, the Johnson–Mehl one, the Poisson mosaic and the dead leaves model. If a Poisson point process is the starting process for all these models, their construction and properties are different. The last one will be presented after the Matheron's Boolean model.

2.3.1. The Voronoi tessellation

To construct a Voronoi tessellation, one sets points p_i according to a Poisson process of density θ. An influence zone X_i corresponds to each point p_i, defined by:

$$X_i = \{x : d(x, p_i) < d(x, p_{j\neq i})\} \quad (6)$$

with: $d(x,p)$, the distance from x to p.

This influence zone is a convex polygon in $\mathbb{R}^2$ (Fig. 1) and a convex polyhedron in $\mathbb{R}^3$.

The simplicity of this model led many authors to use it to describe cellular and granular structures. But the Voronoi tessellation is not infinitely divisible, as a Voronoi tessellation in $\mathbb{R}^3$ does not generate a Voronoi tessellation in $\mathbb{R}^2$.

To compare a plane section of a real structure to a Voronoi model in $\mathbb{R}^2$, some characteristics are at our disposal.[13,23] They are summarized in Table 1. In the case of a Voronoi tessellation in $\mathbb{R}^3$, there exists similar relationships (Table 2). Moreover, the star functions

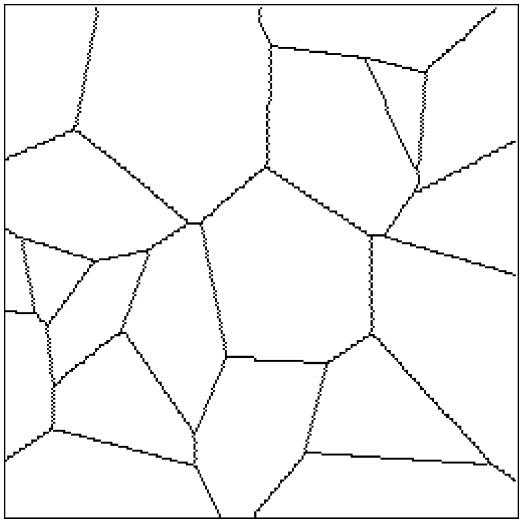

Fig. 1. Voronoi tessellation in $\mathbb{R}^2$ obtained from a skeleton by influence zone (SKIZ) on 20 points.

Table 1
Main characteristics of a tessellation in $\mathbb{R}^2$

Stereological parameters	Mean parameters associated to a cell
Specific perimeter: $L_A(X) = 2\sqrt{\theta}$	Mean surface area: $\bar{A}(X') = \theta^{-1}$
Specific number of cells: $N_A(X) = \theta$	Mean number of vertices: $\bar{P}(X') = 6$
Specific number of vertices: $P_A = 2\theta$	

Table 2
Stereological characteristics of a Voronoi tessellation in $\mathbb{R}^3$

Specific surface area	$S_v = 4\ (\pi/6)^{1/3}\ \Gamma(5/3)\ \theta^{1/3}$
Specific length of triple grain boundaries	$L_v = (16/15)\ (3/4)^{1/3}\ \pi^{5/3}\ \Gamma(4/3)\ \theta^{2/3}$
Specific number of cells	$N_v(X) = \theta$

St_3, St_2, St_1 are related to the Poisson process density θ by the relationships described in Table 3. These star functions are calculated from the moments of the $P(\ell)$ function (which corresponds to the probability that a segment ℓ is included in a given grain[1,3,24]).

2.3.2. Johnson–Mehl tessellation

The Johnson–Mehl tessellation is also based on a point Poisson process. Nevertheless this model is sequential, i.e. function of time.[25] Each sequence dt is made from two elementary processes:

- creation of point nuclei according to a Poisson process of density $\theta = \mu\ \mathrm{d}t$,
- homotopy thinning of nuclei, of thickness $v\ \mathrm{d}t$, according to a rate v.

Nevertheless, all the created nuclei do not necessarily give birth to a "grain". If a nucleus appears in an already grain present, it disappears. This construction stops when the complementary of grains has completely disappeared (Fig. 2). The grains of the tessellation are not always convex, but their characteristics are known and specially the distribution function of the number of neighbours.[23] As in the case of the Voronoi tessellation, the Johnson–Mehl model does not possess stereological

Table 3
Stereological characteristics of tessellation models in $\mathbb{R}^3$

Parameters	Voronoi tessellation	Johnson–Mehl tessellation
Tessellation density in $\mathbb{R}^1$: θ_1	$1.45\ \theta_3^{1/3}$	$1.28\ \theta_3^{1/3}$
Tessellation density in $\mathbb{R}^2$: θ_2	$1.46\ \theta_3^{2/3}$	$1.22\ \theta_3^{2/3}$
Star function in $\mathbb{R}^1$: $St_1(X)$	$0.95\ \theta_3^{-1/3}$	$1.10\ \theta_3^{-1/3}$
Star function in $\mathbb{R}^2$: $St_2(X)$	$1.04\ \theta_3^{-2/3}$	$1.50\ \theta_3^{-2/3}$
Star function in $\mathbb{R}^3$: $St_3(X)$	$1.24\ \theta_3^{-1/3}$	$2.20\ \theta_3^{-1}$

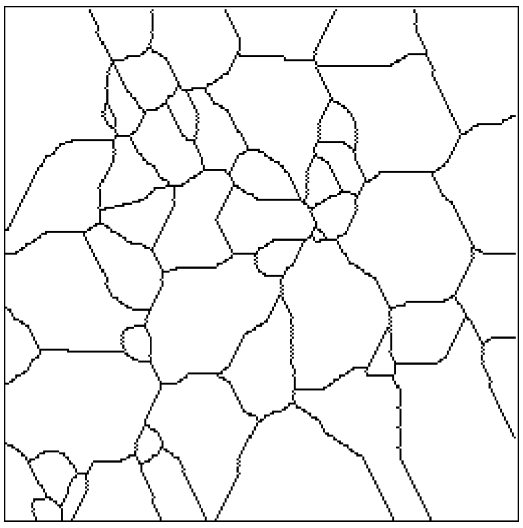

Fig. 2. Johnson–Mehl tessellation in $\mathbb{R}^2$, of size 3, on eight nuclei per sequence.

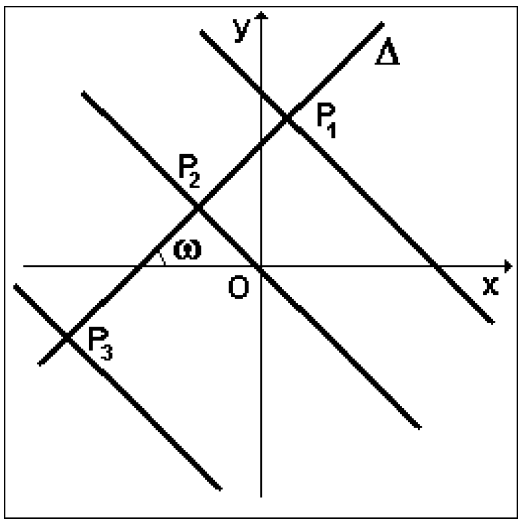

Fig. 3. Construction of a Poisson mosaic.

properties. In the case where μ is constant and, as for the Voronoi tessellation, there exists relationships related to the $P(\ell)$ function, (Table 3).[1,3,24]

2.3.3. Poisson Mosaic

The $\mathbb{R}^2$ space tessellation according to a Poisson process is constructed from Poisson straight lines.[20,26] Let be a straight line Δ with an orientation between ω and $\omega + d\omega$ and going through the origin. On this straight line, a point Poisson process of density $\lambda_2\, d\omega$ is performed (Fig. 3). Through each point, a Poisson straight line perpendicular to Δ is drawn. In the case of an isotropic mosaic, λ is constant and the value of ω is chosen according to a uniform probability law. So the $\mathbb{R}^2$ space is divided in an infinity of random polygons called Poisson polygons (Fig. 4).

A similar construction in $\mathbb{R}^3$ space will lead to a space divided by an infinity of Poisson polyhedra. The ω angle is then between 0 and 2π steradians. The Poisson straight lines are replaced by the Poisson planes perpendicular to Δ, according to a density $\lambda_2\, d\omega$.

Reciprocally to the previous models, the Poisson mosaic possesses stereological properties. On the one hand, the parameter λ_3 of the model characterizes the mean polyhedron, X', by its mean volume, $\bar{V}(X')$, its mean surface area, $\bar{S}(X')$, and its integer of mean curvature, $\bar{M}(X')$. Of course, there are the following relationships:

$$\overline{V}(X') = \frac{6}{\pi^4 \lambda^3} \tag{7}$$

$$\overline{S}(X') = \frac{24}{\pi^3 \lambda^2} \tag{8}$$

$$\overline{M}(X') = \frac{3}{\lambda} \tag{9}$$

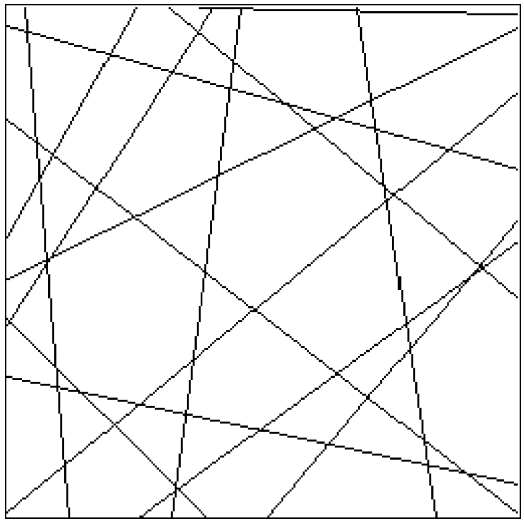

Fig. 4. Poisson mosaic.

On the other hand, a Poisson mosaic in $\mathbb{R}^3$ with a λ_3 parameter, intersected by a plane, generates a Poisson mosaic in $\mathbb{R}^2$ with a λ_2 parameter, and according to:

$$\lambda_2 = \frac{\pi \lambda_3}{2} \tag{10}$$

The Poisson mosaic is rarely used to model a space tessellation. However, it allows to generate random grains for polyphased models.

A last tessellation mode will not be approached here: it is the dead leaves model which will be detailed later on.

2.4. Multiphased RACSs

2.4.1. The Matheron's Boolean model

The most known bi-phased RACS is the Matheron's Boolean model.[1,20,27] To each point of a Poisson process

of density θ, a primary grain is set. The Matheron's Boolean model is the union of all these primary grains (Figs. 5 and 6).

The Matheron's Boolean model possesses very good properties. It is infinitely divisible, stable and calculable. Indeed if X' is the primary grain of the Matheron's Boolean model, there is:

$$Q(K) = \exp\left(-\theta E\left(\mathrm{Mes}\left(X' \oplus \check{K}\right)\right)\right) \tag{11}$$

with: E (Mes $(X' \oplus \check{K})$) the mathematical expectation of the measure of Lebesgue of the set X dilated by the compact K.

Eq. (11) can be written as:

$$Q(\mathrm{K}) = \Pr\left(\mathrm{x} \in \mathrm{X^c} \ominus \check{\mathrm{K}}\right) \tag{12}$$

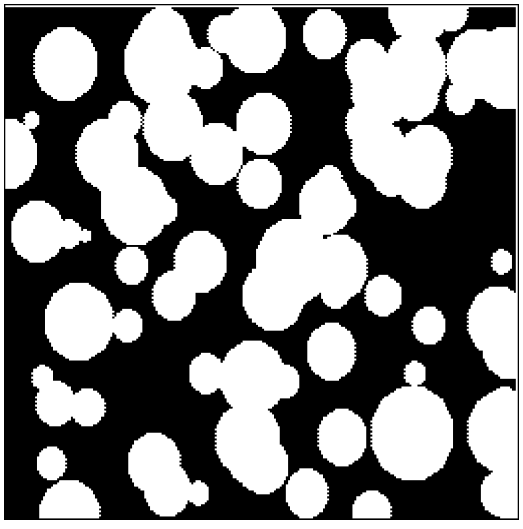

Fig. 5. Matheron's Boolean model with circular disks of normal distribution ($\theta = 80$; $m = 12$; $\sigma = 5$).

Fig. 6. Matheron's Boolean model with Poisson grains ($\theta = 70$; $\lambda' = 35$).

with, $\boldsymbol{X}^{\mathrm{C}} \ominus ; \check{\boldsymbol{K}}$ the erosion of the complementary set of X by the compact K.

To test a Matheron's Boolean model by the Choquet's capacity (or by the complementary functionnal), it is sufficient to estimate the ratio of the eroded by one or several families of compacts, K, each family being defined by the set of self-similarity compacts. A Matheron's Boolean model will be defined by the Poisson density, θ, and the primary grain characterized by a shape and a size distribution.

If the primary grain is convex and with a simple geometry, the Matheron's Boolean model will be calculated from the stereological parameters of the mean grain, X', $\bar{V}(X')$, $\bar{S}(X')$, and $\bar{M}(X')$.

These parameters are already known for Poisson polyhedra [Eqs. (7)–(9)]. In the case of spherical grains, the stereological parameters are calculable from the moments 3, 2 and 1 of the size distribution, $f(a)$. There are the relationships:

$$\overline{V}(X') = \frac{\pi}{6} E\left(a^3\right) \tag{13}$$

$$\overline{S}(X') = \pi E\left(a^2\right) \tag{14}$$

$$\overline{M}(X') = 2\pi E(a) \tag{15}$$

At least, as a union of Matheron's Boolean models gives always a Matheron's Boolean model, many solutions to approach the modelling of a real structure exist.

Some compact sets are particularly interesting to test a Matheron's Boolean model. They are the points ($K = P$), the segments ($K = \ell$), the hexagons of size r ($K = H(r)$), the bi-point ($K = h$), and for some models the triple of points defined by the vertices of an equilateral triangle ($K = T(h)$). For the convex compacts, there are the following relationships:

$$Q(P) = q\exp\left(-\theta \overline{V}(X')\right) \tag{16}$$

$$Q(\ell) = q\exp\left(-\theta \ell \frac{\overline{S}(X')}{4}\right) \tag{17}$$

$$Q(H(r)) = q\exp\left[-\theta\left(-\frac{3r}{4}\overline{S}(X') + \frac{3\sqrt{3}}{8} r^2 \overline{M}(X')\right)\right] \tag{18}$$

For the bi-point ($K = h$), one uses the mean geometrical covariogram, $K(h)$, rather than the covariance, $Q(h)$. The covariogram is related to the covariance by:

$$\frac{K(h)}{K(0)} = 2 - \frac{\mathrm{Log}(Q(h))}{\mathrm{Log}(q)} \tag{19}$$

In the case of Poisson grains, one has:

$$\frac{K(h)}{K(0)} = \frac{K(h)}{\overline{\overline{V}}(X')} = \exp(-\pi\lambda\ell) \tag{20}$$

For spherical grains, the geometrical covariogram is function of the distribution. If a is the maximum size of the primary grain, one has:

$$K(h)\frac{\pi}{6}\left[\int_h^\infty a^3 f(a)\mathrm{d}a - \frac{3h}{2}\int_h^\infty a^2 f(a)\mathrm{d}a + \frac{h^3}{2}\int_h^\infty f(\mathrm{d}a)\right] \tag{21}$$

2.4.2. Dead leaves model

The dead leaves model is a sequential Matheron's Boolean model. Its multiphase version is due to Jeulin.[28] Its construction is as follow: primary grains are generated by a Poisson process of density $\theta(t)$. Conversely to the Matheron's Boolean model, the grains can be overlapped. The first ones can disappear under the second ones and so on. The process can be stopped at time t. If all the support is not completely covered, the process looks like a Matheron's Boolean model. If the process is performed until the stationarity, the support is fully recovered by the tessellation.

In the case of a two-phased dead leaves model the "white" and "black" primary grains appear successively respectively with the densities $\theta_1(t)$ and $\theta_2(t)$. The process is pursued until stationarity, which leads to a two-phased structure where the two phases are imbricated (Figs. 7 and 8). These models are infinitely divisible and, so, generate equivalent models in the sub-sets, when using the same primary grains for every phase. The calculability is not as strong as in the Matheron's Boolean model. The capacities of Choquet are calculable only for $K=h$ and for $K=T(h)$.[28,29] When the bi-point is tested, one uses the function $\varphi(h)$ defined by:

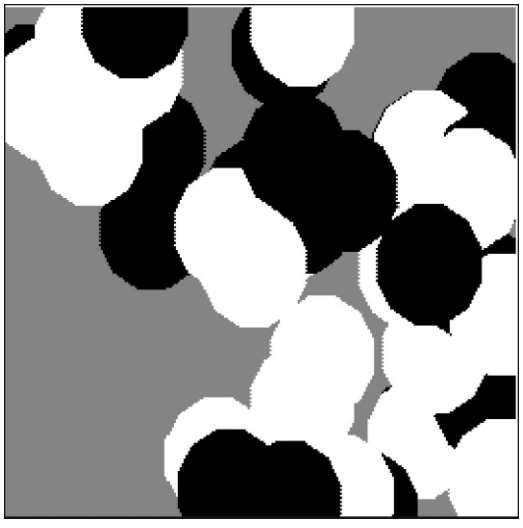

Fig. 7. Construction of a two-phased dead leaves model with circular primary grains in black and white, of size 30 (20 iterations).

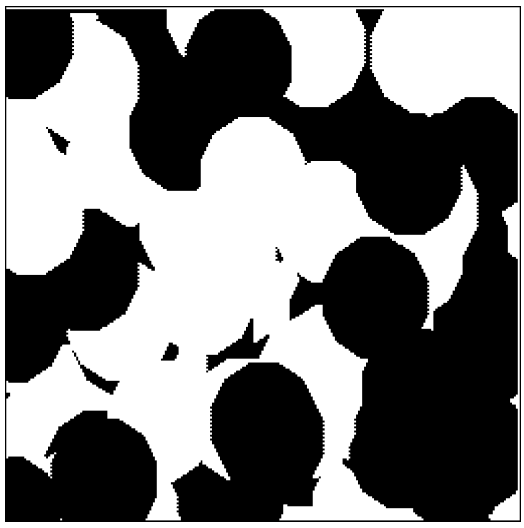

Fig. 8. Model of Fig. 7 until stationarity (density of primary grains in white and black is identical).

$$\varphi(h) = \frac{2 - r_1(h) - r_2(h)}{2 - p \quad r_1(h) - qr_2(h)} \tag{22}$$

with, $r_i(h) = K_i(h)/K_i(0)$.

2.4.3. Tessellation of polyphased space

All the space tessellation can also be used for polyphased space by a random affectation of the classes of the tessellation, called a mosaic model.[8,28]

- *Poisson mosaic*: To obtain a polyphased Poisson tessellation requires first to construct a space tessellation, and to assign the classes to a given phase by a random way. The model parameters are the volume fraction of each phase and λ which characterizes the Poisson tessellation. In the case of a two-phased Poisson mosaic (Fig. 9), the properties of the monophased system are kept. The analytical laws are known for $K=h$, $K=\ell$, and $K=T(h)$:[8,9,29]

$$P(\ell) = p\,\exp(-q\pi\lambda\ell) \tag{23}$$

$$Q(\ell) = q\,\exp(-p\pi\lambda\ell) \tag{24}$$

$$C(h) = \overline{C}(h) + p^2 = p^2 + pq\,\exp(-\pi\lambda\ell) \tag{25}$$

$$\overline{W}(T(h)) = Q(T(h)) - q^3 = -q(1 - 3q + 2q^2)\exp\left(-\frac{3}{2}\pi\lambda h\right) \tag{26}$$

- *Other colored tessellation*: The principle used for the Poisson tessellation can be also utilized for other models of tessellation. Fig. 10 illustrates the case of a two-phased Voronoi tessellation.

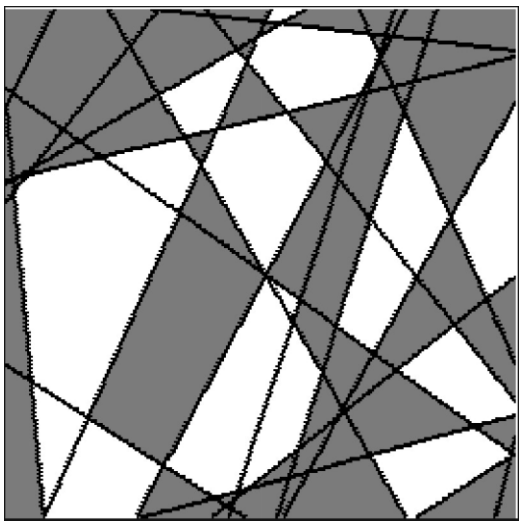

Fig. 9. Mosaic of a two-phased Poisson tessellation.

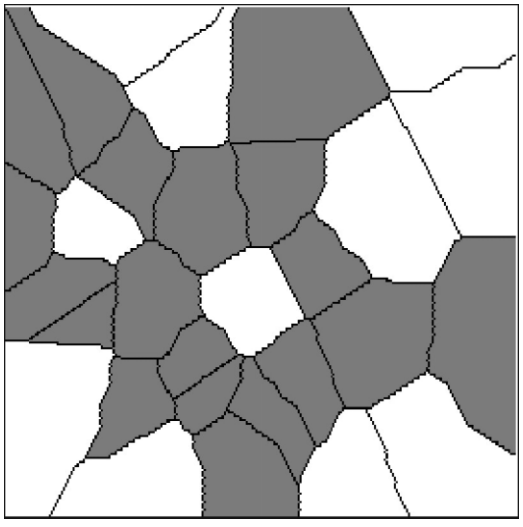

Fig. 10. Two-phased Voronoi tessellation.

2.4.4. Stienen's model

With a Matheron's Boolean model or a dead leaves model, primary grains can be overlapped. To construct the model proposed by Stienen,[30] we still start from a point Poisson process of density θ, but each point is replaced by the largest sphere contained in the corresponding Voronoi tessellation. In these conditions, the spheres are not overlapped, but can be in contact (Fig. 11). It has been generalized in reducing the sphere size by a factor α [0,1]. In the case of the initial model ($\alpha = 1$), the sphere content is constant as one has:

$$Vv(\mathrm{X}) = \left(\frac{\alpha}{2}\right)^3 \tag{27}$$

Moreover, the sphere distribution is known as it is directly related to the distance distribution of the nearest neighbours of a Poisson process, as:

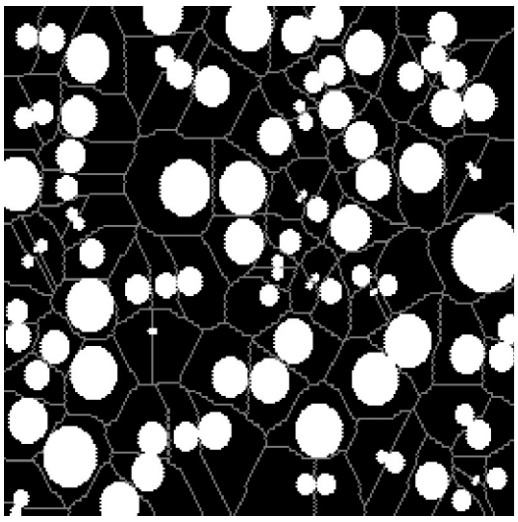

Fig. 11. Model of Steinen in a plane ($\alpha = 1$, $\theta = 100$).

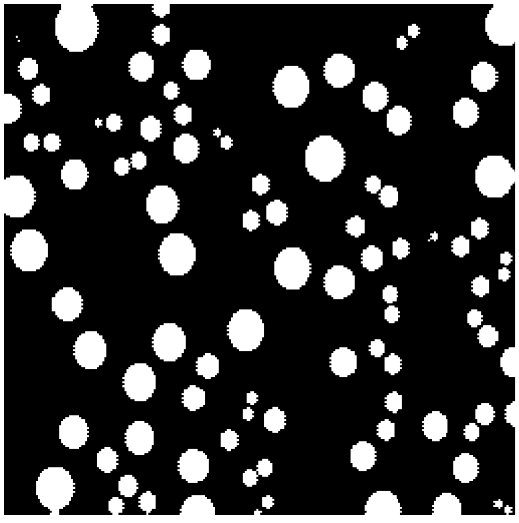

Fig. 12. Generalized model of Steinen in a plane ($\alpha = 0.3$, $\theta = 100$).

$$F(D) = 1 - \exp\left(-\frac{\pi\theta}{6V_{\mathrm{v}}(X)}D^3\right) \tag{28}$$

For $\alpha \neq 1$, the spheres are no more in contact (Fig. 12). The correlation function of a pair of points as a function of the distance, r, can be calculated by numerical integration.[31] Finally for this model, one has at our disposal only a complex expression for the covariance.[32]

3. Some model materials

The materials which can be chosen as model are numerous and various. Some examples mainly based on ceramics will be given, as an illustration.

3.1. Monophased materials

Historically, a Voronoi tessellation or a Johnson–Mehl model were proposed to model the metallic or

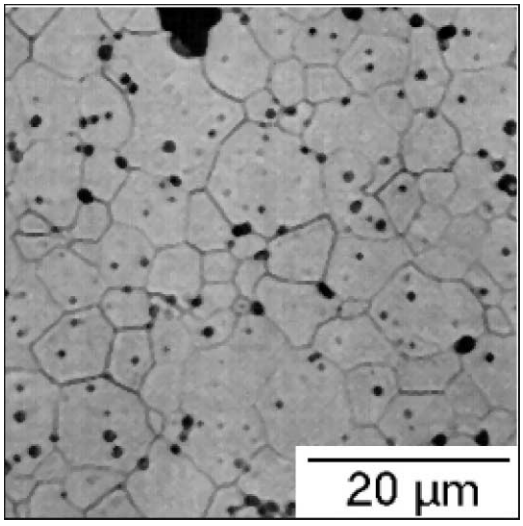

Fig. 13. Optical micrograph of sintered UO_2, after thermal etching.

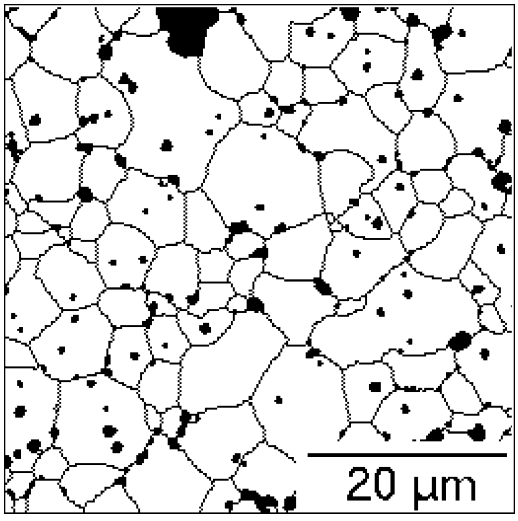

Fig. 14. Binary image of Fig. 13 obtained after filtering, morphological processing and threshold.

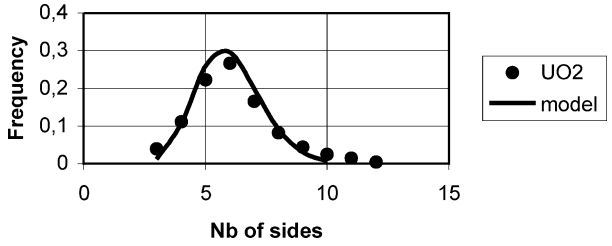

Fig. 15. Theoretical and experimental distribution of the number of sides during the sintering of UO_2.

ceramic polycrystalline microstructures. Tests were also performed on an austenitic steel by comparison with a Voronoi tessellation,[13] but these results were not convincing. The Johnson–Mehl model will be much better suited to explain the existence of non-convex grains. Moreover, the choice of austenite as a model material is not the best one because of a peritectic decomposition which arises during the formation of this phase. A pure metal would be preferable.

Some attempts were made to describe monophased polycrystalline ceramics obtained by sintering. For the case of UO_2 (Figs. 13 and 14) one has compared the experimental distribution of the number of first neighbours with that of the Voronoi theoretical one.[5,33] The agreement is not perfect. But if the porosity is neglected, the structure is approximately described by a Voronoi model. Using Tables 2 and 3, the model could be confirmed or invalidated (Fig. 15).

3.2. Polyphased materials

The book of Matheron,[27] published in 1967, is the starting point of the probabilistic models, with the presentation of the Boolean model, named now Matheron's Boolean model, to describe porous media. It was really used for example to describe metallurgical formed cokes.[29,34] It has also been used to describe two-phased materials obtained by liquid sintering.

- *Fe–Ag system*: Bretheau and Jeulin[35] have investigated the Fe–Ag system. For such materials, a Matheron's Boolean model was tested by comparing the analytical relationships of the segment ℓ, given by Eq. (17) and that given by the bi-point h in Eqs. (19) and (21). A distribution of spherical, uniform or linear, primary grains, permits to correctly modelize this material.
- *WC–Co and TiC–Co cermets*: The same type of analysis has been undertaken in the case of cermets (CERamic METal) fabricated by liquid phase sintering, TiC–Co and WC–Co.[36–39] These two systems differ by the fact that the dispersed phase corresponds either to rounded grains (TiC) or polyedrical grains (WC) (Figs. 16 and 17).

  In the case of TiC–Co (Fig. 16), a dead leave model with spherical grains and a Matheron's Boolean model also with spherical grains have been tested. This last model with spherical primary grains can describe materials sintered, for example, at 1723 K (Fig. 18), but the distribution law of primary grains evolves with the sintering time [Eqs. (19) and (21)]. So, the model does not seem to be perfectly convenient. A precise examination of the simulated and true micrographs shows that the interpenetration of the grains with the Matheron's Boolean model leads to concavities of which only a few exists in the real structure. There is a local rearrangement by coarsening which is not taken into account by the model.

  In the case of WC–Co (Fig. 17), three probabilistic models were tested: a dead leave model with

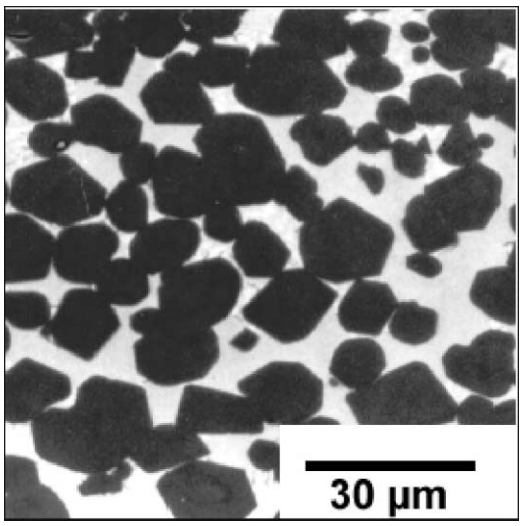

Fig. 16. TiC–Co microstructure.

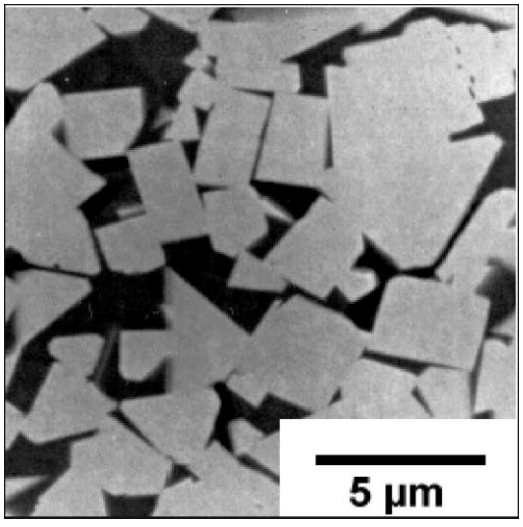

Fig. 17. WC–Co microstructure.

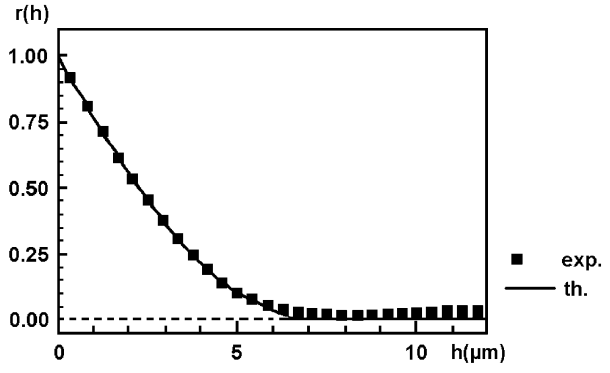

Fig. 18. Theoretical mean geometrical covariogram and experimental points for TiC–Co composites, annealed 4 h at 1723 K.

Poisson grains, a bicolor Poisson mosaic, and a Matheron's Boolean model with Poisson grains. There are three parameters for the dead leave model, the density ratio, θ, of the two types of grains (black and white) and the own characteristics of these two types of Poisson grains, λ_1 and λ_2. The experimental and theoretical functionnals [Eq. (22)] have been compared for the different λ_1 and λ_2 values, but the agreement is not good. Moreover, the simulations show that the phases can form inclusions one inside the other, which is not realistic. So this model must be rejected. As for the bicolor mosaic one, it leads to a unique λ parameter for the two phases (which is not experimentally verified). Moreover the theoretical and experimental connectivity numbers in $\mathbb{R}^2$ confirm these previous results.

So one has compared experimental datæ to the values given by the different analytical laws valid for a Poisson grain Matheron's Boolean model [Eqs. (17), (18) and (20)]. The agreement is excellent. The triple of points given by the following relationship have been tested with success:

$$\mathrm{Log}\left[\frac{Q(T(h))q^3}{Q(h)^3}\right] = q\,\exp\left(-\frac{3}{2}\pi h\right) \tag{29}$$

At least a correct agreement is obtained between the values of the experimental and theoretical numbers of connectivity for the WC phase (Fig. 19).

The Matheron's Boolean model with Poisson grains is verified whatever are the sintering time and temperature. From the estimated parameters of the model, the kinetics law, the rate constant and the activation energy of the sintering process in liquid phase were determined. The obtained results are comparable to those of the literature. But the advantage of the modeling is to permit an

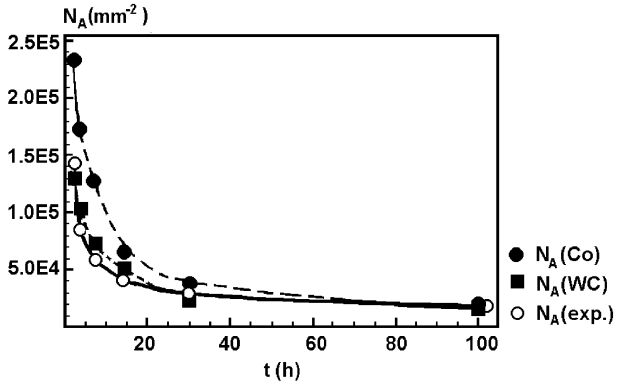

Fig. 19. Comparison between the experimental and theoretical connectivity numbers, N_A, measured on the cobalt (Co) and tungsten carbide (WC) phase for WC–Co, as a function of the sintering time, t.

estimate of the number of connectivity in $\mathbb{R}^3$, $N_V(WC)$, and to inform on its evolution as a function of the cobalt content by a law, which is not possible from classical analysis.

- *Polyphazed ceramic, MOX*: The MOX is a nuclear fuel constituted of about 3–10% of PuO_2, arranged into islands in an UO_2 matrix.[5] For this type of material fabricated by uniaxial pressure of a green mixture, it is interesting to know the spatial distribution of Pu islands. Images of plane sections were obtained by α autoradiography (Fig. 20). To estimate the spatial distribution, the material has been modelized. The autoradiographs show that Pu islands are elliptical, due to the compression stage during the process. A Matheron's Boolean model must describe that material, but we only know the Choquet's relationships for spherical primary grains. So, the strategy was as follows:[33]
  - an affinity is made on the autoradiographs to obtain circular islands ; the affinity ratio is estimated by image analysis from the intercepts in two perpendicular directions (the first one being parallel to the compression axis); that was possible because a Matheron's Boolean model always remains a Matheron's Boolean model after an affinity;
  - so the Choquet's capacity is estimated on an affine image and then compared to the analytical relationships [Eqs. (17), (18) and (21)]; thus, it has been shown that MOX can be described by a Matheron's Boolean model with ellipsoidal primary grains with a log-normal law as a size distribution (Fig. 21);[33]
  - from the estimation of the parameters of the model, the tridimensional structure can be simulated and the distribution between Pu islands calculated (Fig. 22).
- *Concrete*: In the case of concrete, the model is complicated due to several microstructural features. The simplest to solve is the multiphased aspect. The presence of several pertinence scales creates important difficulties. In a first model approach, we shall limit our investigation only to one scale of structure and in $\mathbb{R}^2$ space.

  The investigation of this model material was based on white cement, sand and sieved red gravel to facilitate the segmentation process.[40] In order to simplify the problem, three phases will only be considered: gravel, air-voids and hardened cement paste. The segmentation is based on (i) the decomposition of the color image, (ii) a threshold of gravel by predefined thresholds on the green component of the RGB image and (iii) an automatic threshold of air-voids on the Q component of the color image in the YIQ space.[41] It leads to three binary planes (Fig. 23). The resultant model will be obtained from two primitive models, those of gravel and of air-voids.
- *Gravel model*: Gravel are constituted of grains more or less rounded, separated ones from the

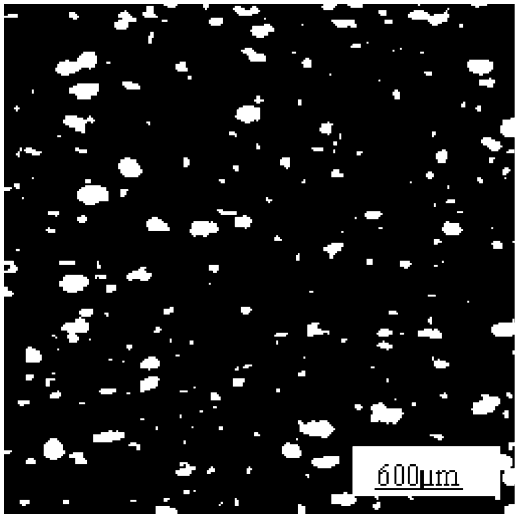

Fig. 20. MOX autoradiograph.

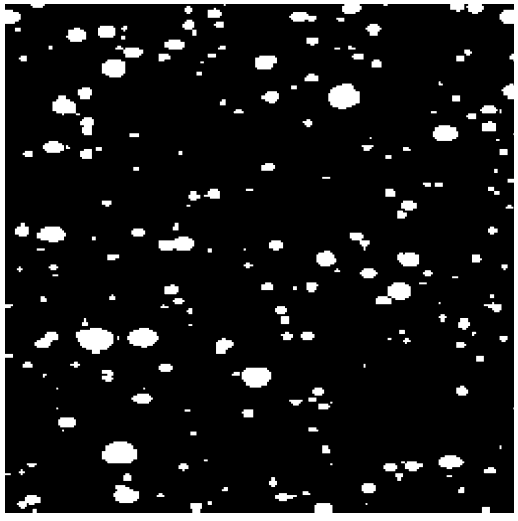

Fig. 21. MOX simulation.

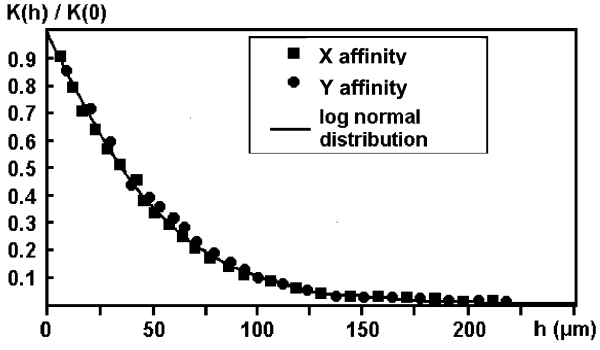

Fig. 22. Comparison between the theoretical and experimental mean geometrical covariogram.

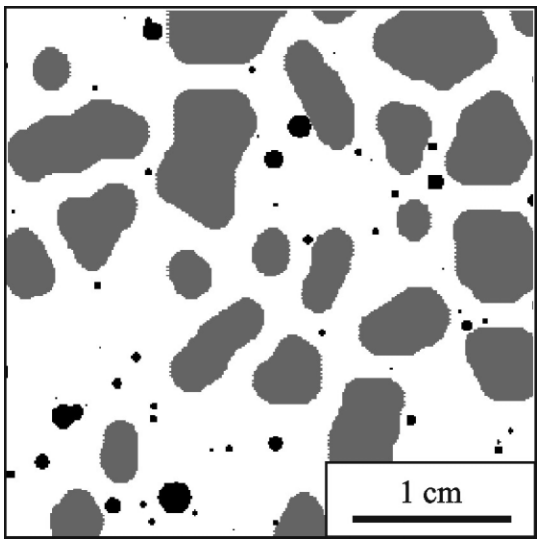

Fig. 23. Real image of a concrete, combining binary planes after segmentation and color image processing, air-voids (in black), gravel (in grey), and cement matrix (in white).

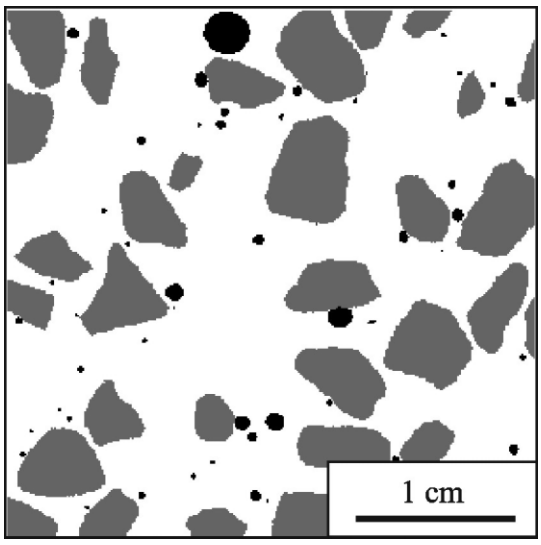

Fig. 24. Simulated image in $\mathbb{R}^2$.

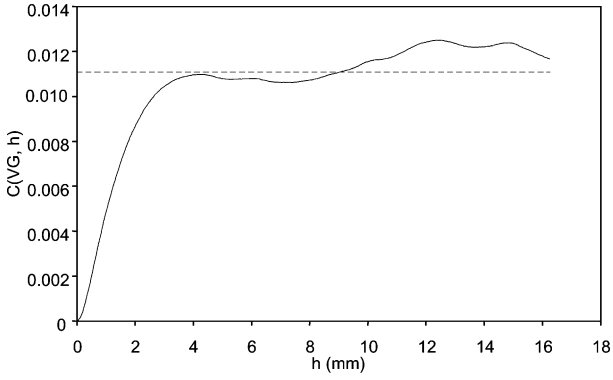

Fig. 25. Crossed covariance of air-voids—gravel on a real structure.

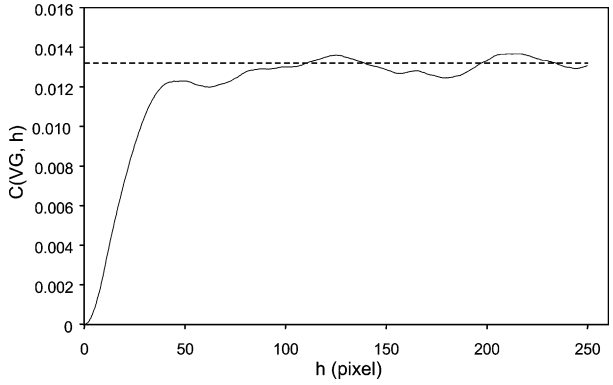

Fig. 26. Crossed covariance of air-voids—gravel on a simulated structure.

others by a hardened cement paste. To obtain such a random structure a Voronoi tessellation is used and then eroded to have disconnected grains, which are polyedral grains. To form rounded grains, an opening of the polyedral structure is used. The threee parameters of this simulation are, the density of the Poisson process, θ,

- the erosion step, λ_1, related to the minimum distance between gravel,
- the opening step, λ_2, related to the minimum curvature of the gravel.

- *Air-voids model*: The structure of the air-voids is represented by a Matheron's Boolean model with spherical grains. As has been previously shown, such a model is completely defined only if the distribution of the primary grains is known. Granulometry investigations of air-voids on real materials follow an exponential law.[40,42] Moreover it is in agreement with the "fractal aspect" described by certain authors for the air-void structure. So one will have a Matheron's Boolean model of air-voids of density θ' with an exponential distribution law of parameters a and b. That is validated by the comparison between the theoretical and experimental Choquet's capacities for the compacts ℓ and H. The mean geometrical covariogram, obtained with h, gives less pertinent results, with a curve slightly below the asymptote, as for the Stienen's model.
- *Concrete model*: Of course, air-voids cannot appear in gravel. Moreover air-void are totally included in the cement paste, they are always included in the hardened cement paste and never in contact with gravel, as it was shown by Dequiedt.[40] So the concrete model is obtained from the combination of the gravel model and the Matheron's Boolean model less the connex component touching gravel (Fig. 24).

To fully validate this 2D model, analytical laws can be used. The model is then compared to real microstructure through crossed-covariance results. Some crossed covariances for air-voids and gravel,

C(VG,h), are presented in Figs. 25 and 26. The general trend of these curves is similar. Moreover, the behavior at the origin is exactly the same. Similar results were also obtained with other crossed covariances.[40,43] This model will be the starting point of a 3D characterization.

4. Conclusion

In this paper, we have presented probabilistic models which are mainly based on closed random sets and tessellations. Of course other types of models exist and have been and are developed: one can quote those based on computer-simulated grain structure,[44–49] on Voronoï cells or mosaic patterns,[49,50] on discrete numerical modelling and packing of spheres,[51,52] even on a microstructural scale, using an image processing based on finite element method (FEM),[53] or …. They describe microstructures more or less correctly. From discrete numerical modelling and packing of spheres, the simulation corresponds to materials made from more or less circular particles. For other materials, one has to change the cellular-automata rules applied to the starting microstructure as it has been made by Bentz for the hydration of Portland cement.[46]

Compared to these results, probabilistic models are well suited for the simulation of ceramic microstructures. They present many advantages as they require few parameters to describe the morphology of a material and that many of them possess stereological properties, that means that you can measure exactly morphological parameters on a section (2D) and obtain, for example, the objects per unit volume without any hypothesis, which can only be measured experimentally by serial sectionning if you do not make hypotheses.

If the model has no interesting stereological properties, the low number of necessary morphological parameters to describe the microstructure and the possibility to use morphological tools to generate the model allow to easily realize 3D simulations which can be used.

We have also shown many uses of these models to describe as well mono-phased as poly-phazed materials. Another field of interest is their uses to simulate non-planar surfaces and to investigate fractured materials.[15–18]

Acknowledgements

This work was performed in the frame of the "Pôle Traitement et Analyse d'Images", Pôle TAI (Pole of Image Processing and Analysis) of Basse-Normandie, France. Concrete specimens were elaborated at ESITC, Groupe ESTP, Epron; we want to thank this School of engineers for allowing us to use their facilities. The authors want to thank their students, Drs. François Charollais, Anne-Sophie Dequiedt and Jean-Louis Quenec'h for presenting some of their results. This paper is the result of many fruitful discussions with our friend Dr. Dominique Jeulin from the Centre de Morphologie Mathématique of the School of Mines of Paris, at Fontainebleau (France); we would like to thank him warmly, and also Dr. Leszek Wojnar from Krakow University (Poland) for the full publication of that paper.

References

1. Serra, J., *ImagE Analysis and Mathematical Morphology*. Academic Press, London, 1982.
2. Serra, J. (ed.), *Image Analysis and Mathematical Morphology*, Vol. 2 *Theoretical Advances*. Academic Press, London, 1988.
3. Coster, M. and Chermant, J. L., *Précis d'Analyse d'Images. Les Presses du CNRS, Paris*, 2nd edn. Les Editions du CNRS, Paris, 1988.
4. Yang, S., Gokhale, A. M. and Shan, Z., Utility of microstructure modelling for simulation of micro-mechanical response of composite containing non-uniformly distributed fibers. *Acta Mater.*, 2000, **48**, 2307–2322.
5. Charollais, F. *Analyse d'Images, un Outil pour Caractériser et Modéliser la Microstructure du Combustible MOX*. Thèse de Doctorat of the University of Caen, 1997.
6. Law, A. M. and Kelton, W. D., *Simulation Modeling and Analysis*, 2nd edn. Mc Graw Hill International Editions, New York, 1991.
7. Matsubara, H., Normura, H. and Kitaoka, S., Design of ceramic microstructures by the Monte Carlo simulations. *Key Eng. Mater.*, 1999, **161-163**, 35–38.
8. Jeulin, D. *Modéles Morphologiques de Structures Aléatoires et de Changement d'Échelle*. Thèse de Docteur ès Sciences, University of Caen, 1991.
9. Jeulin, D., Multivariate random image models. *Acta Stereol.*, 1992, **11**, 59–66.
10. Jeulin, D., Terol Villalobos, I. and Dubus, A., Morphological analysis of UO_2 powder using a dead leaves model. *Micros. Microanal. Microstruct.*, 1995, **6**, 371–384.
11. Jeulin, D. and Squillaci, E. Analyse morphologique de poudres sphériques. In *Colloque sur le Traitement des Poudres et leurs Conséquences*, SF2M, Paris, 18–20 Mars 1996.
12. Jeulin, D., Dead leaves models, from spaces tessellation to random functions. In *Advances in Theory and Applications of Random Sets*, ed. D. Jeulin. World Scientific, Singapore, 1997, pp. 137–156.
13. Stoyan, D., Random sets, models and statistics. *Int. Stat. Rev.*, 1998, **66**, 1–27.
14. Stoyan, D., Kendall, W. S. and Mecke, J., *Stochastic Geometry and its Applications*, 2nd edn. Wiley and Sons, Chichester, 1995.
15. Jeulin, D. and Laurenge, P., Morphological simulation of the roughness transfer on steel sheets. *Microsc. Microanal. Microstruct.*, 1996, **7**, 541–547.
16. Jeulin, D. and Laurenge, P., Simulation of rough surfaces by morphological random functions. *J. Electronic Imaging*, 1997, **6**, 16–30.
17. Aubert, A. and Jeulin, D., Classification morphologique de surfaces rugueuses. *Rev. Met. CIT Sci. Génie Mat.*, 2000, **976**, 247–262.
18. Barré, F. and Lopez, J., Analyse multiéchelle de motifs tridimensionnels sur des surfaces rugueuses. *Rev. Met. CIT Sci. Génie Mat.*, 2000, **97**, 239–246.
19. Mandelbrot, B., *Fractals, Form, Chance and Dimension*. Freeman, San Francisco, 1977.

20. Matheron, G., *Random Sets and Integral Geometry*. Wiley and Sons, New York, 1979.
21. Jeulin, D. (ed) *Advances in Theory and Applications of Random Sets*. World Scientific, Singapore, 1997.
22. Choquet, G., Theory of capacities. *Ann. Inst. Fourier*, 1953, **5**, 131–295.
23. Miles, R. E., The random division of space. *Suppl. Adv. Prob.*, 1972, **4**, 243–266.
24. Haas, A., Matheron, G. and Serra, J., Morphologie mathématique et granulométries en place. *Ann. Mines*, 1967, **11**, 735–753, **12**, 767–782.
25. Johnson, W. A. and Mehl, R. F., Reaction kinetics in processes in nucleation and growth. *Trans. Am. Inst. Min. Eng.*, 1939, **135**, 416–458.
26. Miles, R. E., Poisson flats in euclidean spaces, part 2, Homogeneous Poisson flats and the complementary theorem. *Adv. Prob.*, 1971, **3**, 1–43.
27. Matheron, G., *Eléments pour une Théorie des Milieux Poreux*. Masson, Paris, 1967.
28. Jeulin, D., Multi-component random models for description of complex microstructures. *Mikroscopie*, 1980, **37**, 130–137.
29. Jeulin, D. *Morphologie Mathématique et Propriétés Physiques des Agglomérés de Minerais de fer et de Coke Métallurgique*. Thèse de Docteur-Ingénieur, Ecole Nationale Supérieure des Mines de Paris, Paris, 1979.
30. Steinen, H., The sectionning of randomly dispersed particles, a computer simulation. *Mikroskopie (Wien)*, 1980, **S37**, 74–78.
31. Stoyan, D. and Wiencek, K., Spatial correlation in metal structures and their analysis. *Mater. Charact.*, 1991, **26**, 167–176.
32. Schlater, M. and Stoyan, D., The covariance of the Stienen model. In *Advances in Theory and Applications of Random Sets*, ed. D. Jeulin. World Scientific, Singapore, 1997, pp. 157–174.
33. Charollais, F., Bauer, M., Coster, M., Jeulin, D. and Trotabas, M., Modelling the structure of a nuclear ceramic obtained by solid phase sintering. *Acta Stereol.*, 1997, **16**, 315–321.
34. Jeulin, D., Description du réseau poreux macroscopique de cokes moulés par un modèle morphologique. *Pract. Met.*, 1978, **S8**, 253–263.
35. Bretheau, T. and Jeulin, D., Caractéristiques morphologiques des constituants et comportement à la limite élastique d'un matériau biphasé Fe-Ag. *Rev. Phys. Appl.*, 1989, **24**, 861–869.
36. Quenech, J. L. *Modéles Probabilistes et Frittage en Phase Liquide*. Thèse de Doctorat of the University of Caen, 1994.
37. Quenech, J. L., Coster, M., Chermant, J. L. and Jeulin, D., Study of the liquid phase sintering process by probabilistic models, application to the coarsening of WC–Co cermets. *J. Microscopy*, 1992, **168**, 3–14.
38. Coster, M., Quenec'h, J. L., Chermant, J. L. and Jeulin, D., Probabilistic models and image analysis, tools used to describe liquid phase. In *Probability and Materials, Tests Models Applications Vol. 269.*, ed. D. Breysse. Kluwer, Dordrech, 1994, pp. 403–414 NATO ASI Series E. Applied Sciences.
39. Quenech, J. L., Jeulin, D., Coster, M. and Chermant, J. L., Approach of liquid phase sintering process by probabilistic models. In *Advances in Theory and Applications of Random Sets*, ed. D. Jeulin. World Scientific Pub, Singapore, 1997, pp. 231–249.
40. Dequiedt, A. S., *Contribution à l'Étude Morphologique des Ciments et Bétons par Analyse d'Images Multimodales*. Thèse de Doctorat of the University of Caen, 1999.
41. Kohler, A., A segmentation system based on thresholding. *Comp. Graphic Image Process*, 1981, **15**, 319–338.
42. Dequiedt, A. S., Coster, M., Chermant, L. and Chermant, J. L., Distances between air-voids in concrete by automatic methods. *Cem. Concr. Comp.*, 2000, **22**, 247–254.
43. Dequiedt, A. S., Coster, M., Chermant, J. L. and Jeulin, D., Towards a model of concrete microstructure. *Cem. Concr. Comp*, 2000, **22**, 289–297.
44. Garboczi, E. J. and Bentz, D. P., Computational materials science of cement-based materials. *Mat. Res. Bull.*, 1993, **18**, 50–54.
45. Bentz, D. P., Garboczi, E. J., and Martys, N. S., Application of digital-image based models to microstructure, transport properties, and degradation of cement-based materials. In *The Modelling of Microstructure and its Potential for Studying Transport Properties and Durability*, ed. H. Jennings et al. Kluwer Academic, 1996, pp. 167–185.
46. Bentz, D. P., Three-dimensional computer simulation of Portland cement hydration and microstructure development. *J. Am. Ceram. Soc.*, 1997, **80**, 3–21.
47. Mehnert, K., Ohser, J. and Klimanek, P., Testing stereological methods for the estimation of spatial size distribution by means of computer-simulated grain structures. *Mater. Sci. Eng.*, 1998, **A246**, 207–212.
48. Nippe, M. and Ohser, J., The stereological unfolding problem for systems of homothetic particles. *Patt. Recogn.*, 1999, **32**, 1649–1655.
49. Li, M., Ghosh, S., Richmond, O., Weiland, H. and Rouns, T. N., Three dimensional characterization and modeling of particle reinforced metal matrix composites. Part I, Quantitative description of microstructural morphology. *Mat. Sci. Eng.*, 1999, **A265**, 153–173.
50. Xi, Y., Tennis, P. D. and Jennings, H. M., Mathematical modeling of cement paste microstructure by mosaic pattern, Part I. Formulation. *J. Mater. Res.*, 1996, **11**, 1943–1952.
51. Stroeven, M. *Discrete Numerical Modelling of Composite Materials, Application to Cementious, Materials*. PhD Thesis, Technische Universität Delft, 1999.
52. Dinger, D. R., One-dimensional packing of spheres, part II. *Amer. Ceram. Soc. Bull*, 2000, **79**, 83–91.
53. Gokhale, A. M. and Yang, S., Application of image processing for simulation of mechanical response of multi-length scale microstructures of engineering alloys. *Meter. Mat. Trans A.*, 2000, **A30**, 2369–2381.